Title: Mercury stable isotope composition of lichens and mosses from northern Eurasia

J. E. Sonke[1], V.P. Shevchenko[2], J. Prunier[1], R. Sun[1,3], A.S. Prokushkin[4], and O.S. Pokrovsky[1,5]*

[1] *Géosciences Environnement Toulouse, CNRS/IRD/Université Paul Sabatier Toulouse III, France.*

[2] *Shirshov Institute of Oceanology – Russian Academy of Sciences – Moscow, Russia*

[3] *Institute of Surface-Earth System Science, School of Earth System Science, Tianjin University, 300072 Tianjin, China.*

[4] *Sukachev Institute of Forestry SB RAS, Akademgorodok, Krasnoyarsk, 660036, Russia*

[5] *BIO-GEO-CLIM Laboratory, Tomsk State University, Tomsk, Russia*

* Corresponding author: jeroen.sonke@get.omp.eu

Keywords: stable isotopes, Arctic, terrestrial, vegetation, bryophyte, atmospheric deposition, MDF, MIF, AMDE, heavy metals

Abstract

Mercury (Hg) concentrations in lichens and mosses can be used as surrogates for atmospheric Hg deposition to continental surfaces. In this study we collected and analyzed Hg concentrations and isotopic composition of epiphytic tree lichens and terricolous lichens and mosses from remote locations across the Eurasian Arctic and sub-Arctic (50 to 72° N, 30 to 180° E). Total Hg (THg) concentrations ranged from 13 to 7700 ng g^{-1}. Epiphytic tree lichens had significantly higher median THg levels (243 ng g^{-1}) than terricolous lichens (35 ng g^{-1}) and mosses (74 ng g^{-1}). THg is substantially higher in both tree lichens and terricolous lichens near the Arctic Ocean shore, up to 300 km inland. The combined $\delta^{202}Hg$, $\Delta^{199}Hg$, and $\Delta^{200}Hg$ signatures suggest that the elevated coastal Hg levels are delivered by marine air masses rich in gaseous and particulate oxidized Hg^{II} forms, such as $HgBr_2$. Similar to other vegetation Hg isotope studies, inland terricolous lichen and moss $\Delta^{200}Hg$ are near-zero, indicating a dominant (63%) atmospheric Hg^0 origin, followed by Hg^{II} wet and dry deposition. Inland tree lichens carry more positive $\Delta^{200}Hg$ of 0.15‰, similar to the atmospheric Hg^{II} end-member, suggesting they preferentially accumulate Hg^{II} wet and dry deposition compared to co-located terricolous lichens. Mosses from the European sub-Arctic show low $\delta^{202}Hg$ of -3.1‰, which we speculate to result from regional soil Hg^0 emissions that are re-captured by mosses. Overall, the Hg isotope variability of mosses and lichens reveal latitudinal gradients in Hg deposition pathways and identify preferential Hg^0 or Hg^{II} uptake.

Synopsis: Mercury pollutant levels in Eurasian lichen biomonitors are elevated near the Arctic Ocean due to enhanced deposition of oxidized mercury from marine air masses.

Cover Art

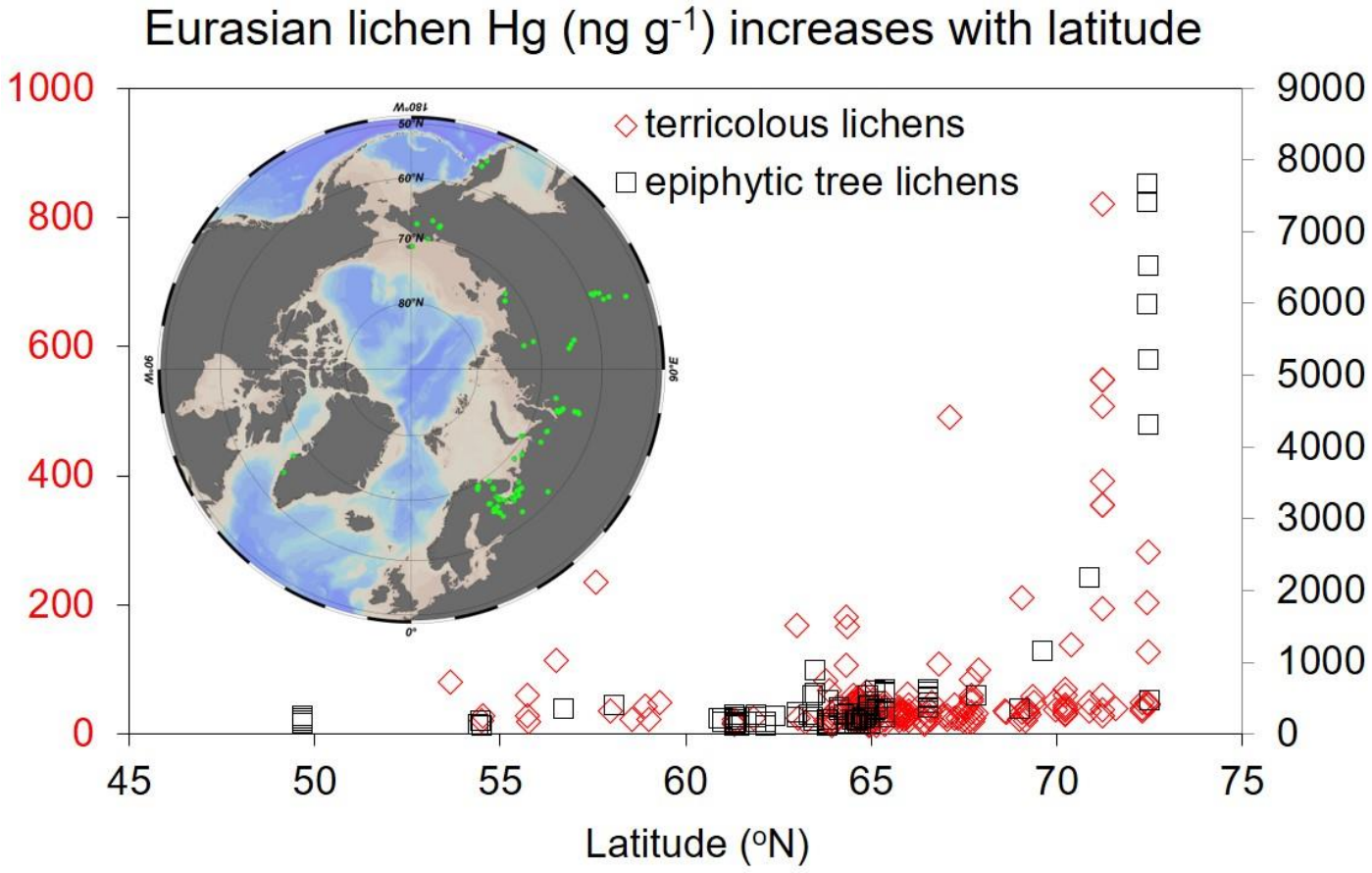
Eurasian lichen Hg (ng g-1) increases with latitude
terricolous lichens
epiphytic tree lichens
1000
800
600
400
200
0
9000
8000
7000
6000
5000
4000
3000
2000
1000
0
45
50
55
60
65
70
75
Latitude (°N)
180°W
50°N
60°N
70°N
80°N
90°W
90°E
0°

Introduction

Present-day anthropogenic Hg emissions (2.4 Gg y^{-1}) to the atmosphere are approximately 7 times larger than natural volcanic and crustal degassing emission (0.34 Gg y-1) [1,2]. Consequently, atmospheric Hg deposition to remote sites has been found to be five to ten times higher than during pre-anthropogenic times [1,3,4]. Increased atmospheric Hg loading to continental watersheds, coastal zones and the open ocean is thought to be one of the key factors responsible for enhanced Hg bioaccumulation in both fresh water and marine food webs [5]. Atmospheric Hg^{II} deposition pathways to terrestrial ecosystems include Hg^{II} wet deposition, via rain and snowfall, Hg^{II} dry deposition, via particle settling and gaseous Hg^{II} scavenging on vegetation and soil surfaces. Vegetation and soils also directly take up gaseous Hg^0 via foliar uptake and sorption [6–8]. The relative importance of these different deposition pathways has traditionally been difficult to constrain.

Hg stable isotope signatures of atmospheric Hg^0 and Hg^{II} pools are sufficiently different so that identification and quantification of deposition pathways becomes possible. In particular, even- (Δ^{200}Hg, Δ^{204}Hg) and odd-Hg (Δ^{199}Hg, Δ^{201}Hg) mass independent isotope fractionation (MIF) signatures contrast in rainfall Hg^{II} from remote locations with Δ^{199}Hg of 0.40‰ and Δ^{200}Hg of 0.17‰, and gaseous Hg^0, with Δ^{199}Hg of -0.20‰ and Δ^{200}Hg of -0.05‰ [9]. Previous studies have examined Δ^{199}Hg and Δ^{200}Hg in tree foliage, mosses, lichens and soil and suggested that a dominant, 75% fraction of vegetation and soil Hg derives from direct vegetation uptake of atmospheric Hg^0 [10–14]. Recent work on permafrost soil Hg concentrations [15–17] and Hg isotopes [18–20] suggested Hg^0 uptake also to be important in Arctic tundra ecosystems. The fate of the permafrost Hg pool under global warming has gained interest [21,22], and understanding pan-Arctic Hg air-vegetation-soil dynamics requires more data on Hg deposition and release pathways in inaccessible remote areas.

Natural vegetation, and in particular lichens and mosses, can act as passive collectors of atmospheric Hg deposition [23–25]. Lichens are symbiotic assemblages of fungi and cyanobacteria or green algae that take up their nutrients mainly from the atmosphere. Soluble and particulate components of dry and wet atmospheric deposition are assimilated by lichen thalli. Thalli surfaces act as ion exchange resins that chelate soluble metals such as Hg. Early studies on lichens from remote locations and urban sites in Canada and Europe revealed negative Δ^{199}Hg of -1.0 to 0.3‰ [26–28]. Later studies on living *sphagnum* moss and *sphagnum* peat accumulations developed a framework where Δ^{200}Hg signatures were used to quantify Hg^{II} wet and dry deposition, and moss Hg^0 uptake [29,30]. Enrico et al. also observed that Δ^{199}Hg in moss and peat showed evidence of minor photochemical foliar Hg^{II} reduction and Hg loss. These observations were extended to Arctic terricolous lichens, showing that even- and odd-Hg MIF provide simultaneous information on Hg deposition and emission [20].

In this study we explore the Hg concentrations and isotopic composition in lichens from the Eurasian (sub-)Arctic. At higher latitudes trees disappear from the permafrost tundra landscape. A comparison was therefore made between epiphyte tree lichens and terricolous lichens on soils. In addition, selected moss species were collected on soils for comparison. While it is often argued that lichens and mosses quantitatively retain atmospheric heavy metal deposition, little is known about the potential re-emission of volatile metals such as Hg from lichen or moss surfaces. The present work provides new insights on these aspects of Hg biogeochemical cycling between the terrestrial and atmospheric compartments, linked via terrestrial vegetation.

Materials and methods

Sampling

Lichen and moss samples were obtained during field campaigns across Siberia from 2004 to 2011 (Figure 1). Two terricolous lichen samples were obtained in SW Greenland in 2007. Epiphyte tree lichens from different *Bryoria, Usnea, Ramalina, Alectoria* and *Evernia* species were collected in trees at 2m height above ground level. Terricolous lichens from different *Cladonia* and *Flavocetraria* species and mosses from *Sphagnum* and *Polytrichum* species were collected at ground level. Moss samples were collected in the White Sea area only, while lichens were collected all across the Eurasian (sub-)Arctic. All samples were transported to the lab, manually cleaned and inspected, and finely ground with a mechanical agate ball mill during 1 minute.

Analyses

All Hg concentration and Hg isotope analyses were performed at the Midi-Pyrenees Observatory in Toulouse, France. Hg concentrations were analyzed in duplicate with a Milestone DMA-80 atomic absorption combustion analyzer. Lichen reference material BCR-482 (480 ± 20 ng g^{-1}, 2σ) was used for quality control, yielding a measured average value of 467 ± 40 ng g^{-1} (2σ, n=17). Hg stable isotopic compositions were analyzed by multi-collector - inductively coupled plasma mass spectrometry (MC-ICPMS, Thermo-Finnigan Neptune) after micro-wave (MARS Explorer) assisted digestion of 100-300 mg powdered lichen in 4 mL of inverse aqua regia (3 mL HNO_3, 1 mL HCl). Digests were diluted to 20 vol% inverse aqua regia and nominal Hg concentrations of 1, 2 or 4 ng g^{-1}. A CETAC HGX-200 cold vapor system and ARIDUS II desolvation unit were used to introduce gaseous Hg^0 and dry aerosol Tl into the MC-ICPMS. Instrumental mass bias was corrected using Tl and the exponential mass fractionation law in a standard-sample-standard bracketing mode. Hg stable isotopic compositions are expressed using the delta notation relative to the NIST SRM 3133 standard:

$$\delta^{xxx}Hg = \left(\frac{\left(\frac{^{xxx}Hg}{^{198}Hg} \right)_{sample}}{\left(\frac{^{xxx}Hg}{^{198}Hg} \right)_{SRM3133}} - 1 \right) \times 1000‰$$

where ^{xxx}Hg represents isotopes other than ^{198}Hg. MIF of the odd Hg isotopes is quantified using the capital delta notation, which amounts to the difference between the observed and the theoretical δ^{xxx}Hg values:

$$\Delta^{xxx}Hg = \delta^{xxx}Hg - \beta_{xxx} \times \delta^{202}Hg$$

where β_{xxx} is the mass dependent scaling factor, e.g. 0.2520 for δ^{199}Hg, 0.5024 for δ^{200}Hg and 0.7520 for δ^{201}Hg [33]. ^{204}Hg was not analyzed. Secondary reference materials UM-Almaden and BCR-482 lichen, processed with each batch of ten samples, were used for quality control (Table 1). UM-Almaden δ^{202}Hg of -0.54 ± 0.09‰, Δ^{199}Hg of -0.03 ± 0.07‰, Δ^{200}Hg of -0.01 ± 0.06‰, Δ^{201}Hg of -0.04 ± 0.09‰ and BCR-482 δ^{202}Hg of -1.59 ± 0.18‰, Δ^{199}Hg of -0.63 ± 0.08‰, Δ^{200}Hg of 0.06 ± 0.06‰, Δ^{201}Hg of -0.64 ± 0.10‰ (mean and 2σ) are in good agreement with published values [33,34]. Uncertainty of sample analysis was considered to be the highest 2σ value observed for UM-Almaden and BCR-482.

Results and Discussion

Hg concentrations

Total Hg (THg, Figure 2a) concentrations in all three sample types are log-normally distributed according to Kolmogorov-Smirnov tests. Median THg levels for mosses are 74 ng g^{-1} (interquartile range (IQR), 53 – 87 ng g^{-1}, n=29), for terricolous lichens 35 ng g^{-1} (IQR, 26 - 49 ng g^{-1}, n=192), for epiphyte tree lichens 260 ng g^{-1} (IQR, 175 – 453 ng g^{-1}, n=113). This range of values is in agreement with a review of forty-three lichen studies in relatively unpolluted or remote sites [23]. A subset of the 334 THg concentrations includes co-located mosses and terricolous lichens in the White Sea area, and co-located terricolous and epiphyte tree lichens across the entire geographical area of study. Kolmogorov-Smirnov testing indicates that Hg concentrations in both co-located data sets are significantly different at the $p<0.001$ level. Therefore, the variable median THg levels of 35, 74 and 260 ng g^{-1} for terricolous lichens, mosses, and epiphyte tree lichens are likely related to a combination of ecological and Hg depositional factors.

Lichen THg concentrations increase as a function of latitude for both epiphyte tree and terricolous species (Figure 2a). Maximum epiphyte tree lichen THg reaches 7700 ng g^{-1} in the Taimyr Peninsula at 72.43 ^{o}N, 101.98 ^{o}E, an area that lies 200 km southwest of the Khatanga river estuary, on the AO. Lichen THg contents at remote background sites globally rarely exceed 400 ng g^{-1} [23]. Epiphyte tree lichen THg in excess of 400 ng g^{-1} occurs at 29 other locations, the majority of which are at latitude >63^{o} N, from 33^{o} E to 123^{o} E, and generally within 300km of the AO coastline. Terricolous lichen THg, while overall lower, also

shows maximum levels at high latitude, reaching 300 – 800 ng g^{-1} from 67 – 79 ^{o}N on Wrangel Island; Medvejii Island and Taimyr Peninsula, all in proximity of the Arctic Ocean. High atmospheric Hg deposition to snow covered sea-ice has been observed repeatedly during spring time atmospheric Hg depletion events (AMDEs) [35,36]. AMDEs occur during polar sunrise when photochemistry of sea-ice, snow on ice, and sea-water derived bromide ions generates bromine radicals that oxidize a large fraction of atmospheric Hg^0 in the polar marine boundary layer [37]. Arctic Ocean air masses containing high Br levels have been observed to penetrate substantially into Siberia, including over the Taimyr Peninsula [38]. Consequently; the influence of AMDEs has been detected inland as far as 200 km of the coast [19], and AMDEs deposit important amounts of atmospheric oxidized Hg^{II} to snow on sea-ice and land. Epiphytic tree lichens sampled along a gradient from Hudson Bay, a salt water body, showed inland decreasing Br and Hg concentrations (up to 2080 ng g^{-1}), reaching background levels only after 600 km, and were suggested to reflect AMDE affected air masses and Hg deposition [39]. Similarly, St Pierre et al. observed elevated Hg up to 361 ng g^{-1} in terricolous coastal lichens of the high Canadian Arctic [40]. Older studies also find elevated Hg up to 927 ng g^{-1} in terricolous coastal lichens in Antarctica [25]. We therefore hypothesize that the elevated THg level in epiphytic and terricolous lichens across coastal Siberia is related to springtime AMDEs and Hg^{II} deposition. In the following, we will use Hg isotopes to further investigate this hypothesis. Lichen THg levels were not correlated with longitude, altitude, or lichen species type. Moss samples were from a more restricted area near the White Sea in European Russia, and did not show unusually elevated THg contents (median 74 ng g^{-1}), compared to European mid-latitude background sites in Spain (40 – 90 ng g^{-1}; [41]) and France (24 – 91 ng g^{-1}; [29]).

Hg stable isotopes

Hg MIF. The Hg stable isotope composition of the (sub-)Arctic lichens and mosses ranges from -5.7 to 0.4‰ for δ^{202}Hg, -1.0 to 0.9‰ for Δ^{199}Hg, and -0.05 to 0.21‰ for Δ^{200}Hg. This wide variability encompasses that of all previously published lichen data (Figure 3). Odd-MIF data define a $\Delta^{199}Hg/\Delta^{201}Hg$ slope of 1.05 (Figure 3c), which is typical of aqueous inorganic Hg^{II} photoreduction observed during experiments and in the natural environment [42,43]. Similar to previous work [18,29], we use Δ^{200}Hg to identify the contribution of atmospheric Hg^{II} wet and dry deposition, and foliar Hg^0 gas uptake. These atmospheric Hg^{II} and Hg^0 pools have contrasting Δ^{200}Hg of 0.14‰ (median; IQR 0.10 to 0.20), and -0.05‰ (median; IQR -0.08 to -0.03) respectively ([9], Table 1). Δ^{200}Hg in tree lichens (median 0.15‰; interquartile range (IQR) 0.11 to 0.18‰) are systematically higher than Δ^{200}Hg in terricolous lichens (0.02‰; -0.01 to 0.06‰), mosses (0.03‰; 0.00-0.05‰), and the group of coastal tree lichens (-0.02‰; -0.03 to 0.01‰), with THg > 900 ng g^{-1}, that is potentially impacted by AMDEs. Continental tree lichens therefore appear to scavenge predominantly the atmospheric Hg^{II} end-member, either in the form of rainfall Hg^{II} or as aerosol and gaseous Hg^{II}. Terricolous lichens and mosses have lower Δ^{200}Hg, closer to the Hg^0 end-member, and similar to observations in the Pyrenees, France and Alaska, USA (Figure 3a). This suggests that foliar Hg^0 uptake is

the dominant Hg sequestration pathway in terricolous lichens and mosses and amounts to 66 and 60% respectively, based on the above atmospheric Δ^{200}Hg end-members.

We observe that tree lichens that scavenged large amounts of atmospheric Hg during AMDEs have unusually low Δ^{200}Hg of -0.02‰ (Figure 3a). The likely reason for this is that the Hg^{II} forms scavenged were produced regionally or even locally, in the polar boundary layer, by Br-oxidation of ambient northern hemispheric Hg^0, with low Δ^{200}Hg of -0.05‰. In other words, during AMDEs Hg^{II} inherits its low Δ^{200}Hg signature directly from Hg^0. This is not the case for Hg^{II} in rainfall and dry deposition which is estimated to be predominantly formed in the middle and upper free troposphere [44] where an unknown photochemical reaction, possibly photoreduction [45], causes even Hg-MIF and generates opposite sign Δ^{200}Hg in the global free tropospheric Hg^0 and Hg^{II} pools.

Within the lichen and moss dataset, the variability of Δ^{199}Hg (Figure 2c) has in common with Δ^{200}Hg that the Hg^{II} and Hg^0 deposition pathways control the initial Δ^{199}Hg magnitude [11]. Atmospheric Hg^{II} and Hg^0 end-members carry opposite Δ^{199}Hg of 0.38‰ and -0.21‰ (Table 1). However, unlike Δ^{200}Hg which is invariant during surface earth photoreduction and re-emission processes, Δ^{199}Hg may further evolve within biota. Evidence for this was shown for mosses, where observed Δ^{199}Hg was lower than that expected from atmospheric end-member mixing [29]. Similarly, in the marine environment intra-cellular photoreduction of Hg^{II} leaves behind residual Hg^{II} that is depleted in odd Hg isotopes, with lower Δ^{199}Hg [46]. AMDE-affected tree lichens also have lower than expected Δ^{199}Hg, and therefore show evidence of photoreductive odd-Hg MIF (Figure 4b). This deficit in odd-Hg isotopes is similar to that observed in snow Hg^{II} during AMDEs [47] (Figure 4b). Mosses, on the contrary show little evidence of post-depositional odd-Hg MIF as their Δ^{199}Hg values are those expected from their Δ^{200}Hg and the Δ^{199}Hg:Δ^{200}Hg ratio of the atmospheric end-members. Half of terricolous lichens also do not show post-depositional odd-Hg MIF, but the other half does with both enhanced Δ^{199}Hg or lower than expected Δ^{199}Hg. Altogether, this suggests that the chemical Hg^{II} compounds (e.g. $HgBr_2$) that deposit on the surface of epiphyte tree lichens and some terricolous lichens readily undergo photoreductive re-emission, either before or after deposition. This photoreduction modifies the Δ^{199}Hg signature, but not Δ^{200}Hg. In contrast, the Hg^0 absorbed during intra-cellular uptake, and the Hg^{II} compounds supplied by rainfall and snowfall to terricolous lichens and mosses (typically consisting of strong Hg^{II}-organic matter complexes [48]) seem less amenable to photoreductive re-emission and odd-MIF. Across the tree lichen dataset, notable latitudinal Δ^{199}Hg and Δ^{200}Hg gradients of -0.033‰ and -0.005‰ per degree (from 49.7 to 72.5° N) are observed (Figure 2c,d), driven by the AMDE Hg deposition dynamics to tree lichens.

Hg MDF. δ^{202}Hg in the (sub-)arctic lichen and moss dataset spans a large range from -5.7 to 0.4‰. δ^{202}Hg of tree lichens have the most positive values, with medians of -0.38‰ and 0.14‰ for continental and AMDE groups respectively. Above we suggested, based on Δ^{200}Hg, that tree lichens scavenge

predominantly atmospheric Hg^{II} forms, e.g. $HgBr_2$. The median $\delta^{202}Hg$ of tree lichens overlaps with the broad $\delta^{202}Hg$ composition of northern hemisphere rainfall Hg^{II}, and Hg^0 (the precursor of AMDE Hg^{II}), suggesting that scavenging of atmospheric gaseous or aerosol Hg^{II} forms does not lead to measurable MDF. Tree lichens impacted by AMDEs in the Hudson Bay also showed relatively high median $\delta^{202}Hg$ of -0.29‰ [27](Figures 3a,b).

Terricolous lichen and moss $\delta^{202}Hg$ are lower with median values of -1.25‰ and -3.10‰ respectively, and a number of even lower, but also higher, outlying values occur (Figures 2b, 3a,b). Even for co-located terricolous and tree lichen samples from the White Sea area, the $\delta^{202}Hg$ difference is observed, suggesting species-specific control factors. Vegetation Hg^0 uptake via stomata and directly through the cuticle surface tissue layers is accompanied by strong, possibly diffusional, MDF of 2-3‰ [29,49]. The final $\delta^{202}Hg$ of lichens and mosses is therefore determined by the $\delta^{202}Hg$ of the local atmospheric Hg^0 pool, the proportion of Hg^0 uptake compared to Hg^{II} scavenging, and the exact MDF factor which is likely species and climate dependent. Any post-depositional reductive Hg loss from lichens and mosses can induce a shift in the residual Hg towards heavier $\delta^{202}Hg$, yet such losses are thought to be minor [20,29]. Terricolous lichen median $\delta^{202}Hg$ of -0.75‰ observed in northern Alaska are similar to our Eurasian lichen data (Figure 3a,b). Mosses from the White sea region also have unusually low median $\delta^{202}Hg$ (-3.1‰) compared to moss $\delta^{202}Hg$ in the French Pyrenees of -1.6‰ [29] and -1.5‰ [50]. Any potential explanation for the low moss $\delta^{202}Hg$ should therefore address both the $\delta^{202}Hg$ difference with co-located lichens, and with the French moss observations.

In Figure 4c we explore a $\delta^{202}Hg$ vs 1/THg source mixing diagram, which shows that, to first order, a high concentration Hg pool with low $\delta^{202}Hg$, and a low concentration Hg pool with high $\delta^{202}Hg$ are potentially involved. In this diagram, three outliers for terricolous and tree lichens, with negative $\delta^{202}Hg$ <4‰ also align on the mixing trend. We suggest that the mosses assimilate a specific atmospheric Hg^0 pool of low $\delta^{202}Hg$. This pool, which dominates the overall isotope composition of moss, appears to have a $\Delta^{200}Hg$ on the order of 0.03‰, $\Delta^{199}Hg$ of 0.07‰, and $\delta^{202}Hg$ of -3.1‰. Preliminary Hg isotope observations of the Yenisei River dissolved Hg, which represents the watershed integrated soil Hg-organic carbon pool typical of West-Siberia, show very similar mean $\Delta^{200}Hg$ of 0.04‰, $\Delta^{199}Hg$ of 0.14‰, and $\delta^{202}Hg$ of -3.0‰ (n=7, [51]). We therefore suggest that the White Sea area mosses have sequestered Hg^0 re-emitted from regional soils. Visibly, terricolous lichens in the same area are less efficient in sequestering Hg^0 than mosses. Overall, we speculate that epiphyte tree lichens and above ground canopy preferentially intercept Hg^{II} dry and wet deposition, leaving less of this pool to be scavenged by near surface terricolous lichens and mosses that are, in addition, covered by snow during the AMDE season. In in-land tree lichens, this leads to elevated $\Delta^{200}Hg$ dominated by Hg^{II} deposition. Terricolous lichens and mosses growing on the active soil layer appear to assimilate relatively larger amounts of Hg^0 than tree lichens, in part originating from soil Hg^0 re-emissions, as indicated by the near-zero $\Delta^{200}Hg$ and negative $\delta^{202}Hg$. Co-located terricolous lichens and

mosses suggest that mosses are more efficient in sequestering Hg^0, leading to higher THg concentrations and more negative $\delta^{202}Hg$.

Perspectives

Our survey of the Hg concentration and isotope composition of Eurasian lichens and mosses reveals significant geographical and physiological differences. Hg concentrations are substantially higher in lichens near the Arctic Ocean shore, up to 300km inland. The combined $\delta^{202}Hg$, $\Delta^{199}Hg$, and $\Delta^{200}Hg$ suggest that the elevated Hg levels are delivered by marine air masses rich in oxidized Hg^{II} forms, such as $HgBr_2$. Across the dataset, a notable latitudinal $\Delta^{199}Hg$ gradient of -0.03‰ per degree is observed. It will be of interest to investigate if this gradient is imprinted on soil Hg, and whether it can be used to monitor northern soil Hg mobilization induced by global warming.

Similar to other vegetation Hg isotope studies, terricolous lichen and moss $\Delta^{200}Hg$ are slightly positive, indicating a dominant (63%) atmospheric Hg^0 origin, followed by Hg^{II} wet and dry deposition. Mosses in the White Sea area show unusually low $\delta^{202}Hg$, which we speculate to result from regional soil Hg^0 emissions that are re-captured by mosses, and less so by co-located lichens. Large variations across the Hg isotope dataset reflect complex air-vegetation-soil Hg cycling and call for dedicated studies over the latitudinal and biome gradients.

Acknowledgements

This work was supported by research grants ANR-09-JCJC-0035-01 from the French Agence Nationale de Recherche and ERC-2010-StG_20091028 from the European Research Council to JES. OP acknowledges support from the Tomsk State University Development Program “Priority-2030”. Jean-Baptiste Bories, Lara Sassine, Cyril Zouiten and Jérôme Chméleff are thanked for Hg concentration analyses and mass spectrometry assistance and Andrey V. Apletalin, Ivan N. Bolotov, Andrey N. Boltunov, Andrey Yu. Bychkov, Anna L. Chultsova, Svetlana I. Drovnina, Svetlana Yu. Evgrafova, Alexander R. Gruzdev, Ildar A. Kal’ko, Nikita V. Kucheruk, Stanislav A. Kutenkov, Natalya M. Makhnovich, Rinat M. Manasypov, Dmitry A. Philippov, Boris G. Pokrovsky, Olga B. Pokrovskaya, Elena A. Rai, Tatyana V. Romanis, Maria I. Rusanova, Alexander S. Savvichev, Liudmila S. Shirokova, Anna A. Soboleva, Dina P. Starodymova, Mikhail V. Stoikin, Dmitry A. Subetto, Marianna I. Tuchkova, Elena V. Vatrushkina, Natalya E. Zaretskaya, Natalya S. Zamber, Natalya A. Zubrii for collection of lichens and moss samples.

References

(1) Li, C.; Sonke, J. E.; Le Roux, G.; Piotrowska, N.; Van der Putten, N.; Roberts, S. J.; Daley, T.; Rice, E.; Gehrels, R.; Enrico, M.; Mauquoy, D.; Roland, T. P.; De Vleeschouwer, F. Unequal Anthropogenic Enrichment of Mercury in Earth's Northern and Southern Hemispheres. *ACS Earth Space Chem.* **2020**, *4* (11), 2073–2081. https://doi.org/10.1021/acsearthspacechem.0c00220.

(2) Streets, D. G.; Horowitz, H. M.; Jacob, D.; Lu, Z.; Levin, L.; ter Schure, A. F. H.; Sunderland, E. M. Total Mercury Released to the Environment by Human Activities. *Environmental Science & Technology* **2017**, *51* (11), 5969–5977. https://doi.org/10.1021/acs.est.7b00451.

(3) Amos, H. M.; Sonke, J. E.; Obrist, D.; Robins, N.; Hagan, N.; Horowitz, H. M.; Mason, R. P.; Witt, M.; Hedgecock, I. M.; Corbitt, E. S.; Sunderland, E. M. Observational and Modeling Constraints on Global Anthropogenic Enrichment of Mercury. *Environmental Science & Technology* **2015**, *49* (7), 4036–4047. https://doi.org/10.1021/es5058665.

(4) Outridge, P. M.; Mason, R. P.; Wang, F.; Guerrero, S.; Heimbürger-Boavida, L. E. Updated Global and Oceanic Mercury Budgets for the United Nations Global Mercury Assessment 2018. *Environ. Sci. Technol.* **2018**, *52* (20), 11466–11477. https://doi.org/10.1021/acs.est.8b01246.

(5) UNEP. Global Mercury Assessment 2018. UNEP Chemicals Branch, Geneva, Switzerland. **2018**.

(6) Jiskra, M.; Sonke, J. E.; Obrist, D.; Bieser, J.; Ebinghaus, R.; Myhre, C. L.; Pfaffhuber, K. A.; Wangberg, I.; Kyllonen, K.; Worthy, D.; Martin, L. G.; Labuschagne, C.; Mkololo, T.; Ramonet, M.; Magand, O.; Dommergue, A. A Vegetation Control on Seasonal Variations in Global Atmospheric Mercury Concentrations. *NATURE GEOSCIENCE* **2018**, *11* (4), 244+. https://doi.org/10.1038/s41561-018-0078-8.

(7) Zhou, J.; Obrist, D.; Dastoor, A.; Jiskra, M.; Ryjkov, A. Vegetation Uptake of Mercury and Impacts on Global Cycling. *Nature Reviews Earth & Environment* **2021**, *2* (4), 269–284. https://doi.org/10.1038/s43017-021-00146-y.

(8) Obrist, D.; Roy, E. M.; Harrison, J. L.; Kwong, C. F.; Munger, J. W.; Moosmüller, H.; Romero, C. D.; Sun, S.; Zhou, J.; Commane, R. Previously Unaccounted Atmospheric Mercury Deposition in a Midlatitude Deciduous Forest. *Proceedings of the National Academy of Sciences* **2021**, *118* (29). https://doi.org/10.1073/pnas.2105477118.

(9) Jiskra, M. Mercury Stable Isotopes Constrain Atmospheric Sources to the Ocean. *Nature* **2021**, *597*, 678–682.

(10) Demers, J. D.; Blum, J. D.; Zak, D. R. Mercury Isotopes in a Forested Ecosystem: Implications for Air-Surface Exchange Dynamics and the Global Mercury Cycle. *Global Biogeochemical Cycles* **2013**, *27* (1), 222–238. https://doi.org/10.1002/gbc.20021.

(11) Enrico, M.; Le Roux, G.; Marusczak, N.; Heimbürger, L.-E.; Claustres, A.; Fu, X.; Sun, R.; Sonke, J. E. Atmospheric Mercury Transfer to Peat Bogs Dominated by Gaseous Elemental Mercury Dry Deposition. *Environmental Science & Technology* **2016**. https://doi.org/10.1021/acs.est.5b06058.

(12) Enrico, M.; Le Roux, G.; Heimburger, L.-E.; Van Beek, P.; Souhaut, M.; Chmeleff, J.; Sonke, J. E. Holocene Atmospheric Mercury Levels Reconstructed from Peat Bog Mercury Stable Isotopes. *Environmental Science & Technology* **2017**, *51* (11), 5899–5906. https://doi.org/10.1021/acs.est6b05804.

(13) Jiskra, M.; Sonke, J. E.; Agnan, Y.; Helmig, D.; Obrist, D. Insights from Mercury Stable Isotopes on Terrestrial-Atmosphere Exchange of Hg(0) in the Arctic Tundra. *Biogeosciences* **2019**, *16* (20), 4051–4064. https://doi.org/10.5194/bg-16-4051-2019.

(14) Zheng, W.; Obrist, D.; Weis, D.; Bergquist, B. A. Mercury Isotope Compositions across North American Forests. *Global Biogeochemical Cycles* **2016**, *30* (10), 1475–1492. https://doi.org/10.1002/2015GB005323.

(15) Lim, A. G.; Jiskra, M.; Sonke, J. E.; Loiko, S. V.; Kosykh, N.; Pokrovsky, O. S. A Revised Northern Soil Hg Pool, Based on Western Siberia Permafrost Peat Hg and Carbon Observations. *Biogeosciences* **2020**, *2020*, 1–35. https://doi.org/10.5194/bg-2019-483.

(16) Olson, C.; Jiskra, M.; Biester, H.; Chow, J.; Obrist, D. Mercury in Active-Layer Tundra Soils of Alaska: Concentrations, Pools, Origins, and Spatial Distribution. *Global Biogeochemical Cycles*. 2018, p doi: 10.1029/2017GB005840.

(17) Schuster, P. F.; Schaefer, K. M.; Aiken, G. R.; Antweiler, R. C.; Dewild, J. F.; Gryziec, J. D.; Gusmeroli, A.; Hugelius, G.; Jafarov, E.; Krabbenhoft, D. P.; Liu, L.; Herman-Mercer, N.; Mu, C.; Roth, D. A.; Schaefer, T.; Striegl, R. G.; Wickland, K. P.; Zhang, T. Permafrost Stores a Globally Significant Amount of Mercury. *GEOPHYSICAL RESEARCH LETTERS* **2018**, *45* (3), 1463–1471. https://doi.org/10.1002/2017GL075571.

(18) Jiskra, M.; Sonke, J. E.; Agnan, Y.; Helmig, D.; Obrist, D. Insights from Mercury Stable Isotopes on Terrestrial-Atmosphere Exchange of Hg(0) in the Arctic Tundra. *Biogeosciences* **2019**, *16* (20), 4051–4064. https://doi.org/10.5194/bg-16-4051-2019.

(19) Obrist, D.; Agnan, Y.; Jiskra, M.; Olson, C. L.; Colegrove, D. P.; Hueber, J.; Moore, C. W.; Sonke, J. E.; Helmig, D. Tundra Uptake of Atmospheric Elemental Mercury Drives Arctic Mercury Pollution. *Nature* **2017**, *547* (7662), 201-+. https://doi.org/10.1038/nature22997.

(20) Olson, C. L.; Jiskra, M.; Sonke, J. E.; Obrist, D. Mercury in Tundra Vegetation of Alaska: Spatial and Temporal Dynamics and Stable Isotope Patterns. *Science of the Total Environment* **2019**, *660*, 1502–1512. https://doi.org/10.1016/j.scitotenv.2019.01.058.

(21) Lim, A. G.; Sonke, J. E.; Krickov, I. V.; Manasypov, R. M.; Loiko, S. V.; Pokrovsky, O. S. Enhanced Particulate Hg Export at the Permafrost Boundary, Western Siberia. *Environmental Pollution* **2019**, *254*, 113083. https://doi.org/10.1016/j.envpol.2019.113083.

(22) Schaefer, K.; Elshorbany, Y.; Jafarov, E.; Schuster, P. F.; Striegl, R. G.; Wickland, K. P.; Sunderland, E. M. Potential Impacts of Mercury Released from Thawing Permafrost. *Nature Communications* **2020**, *11* (1), 4650. https://doi.org/10.1038/s41467-020-18398-5.

(23) Garty, J. Biomonitoring Atmospheric Heavy Metals with Lichens: Theory and Application. *Critical Reviews in Plant Sciences* **2001**, *20* (4), 309–371.

(24) Shevchenko, V. P.; Pokrovsky, O. S.; Starodymova, D. P.; Vasyukova, E. V.; Lisitzin, A. P.; Drovnina, S. I.; Zamber, N. S.; Makhnovich, N. M.; Savvichev, A. S.; Sonke, J. Geochemistry of Terricolous Lichens in the White Sea Catchment Area. *Doklady Earth Sciences* **2013**, *450* (1), 514–520. https://doi.org/10.1134/S1028334X13050073.

(25) Bargagli, R.; Battisti, E.; Focardi, S.; Formichi, P. Preliminary Data on Enviornmental Distribution of Mercury in Northern Victoria Land, Antarctica. *Antarctic Science* **1993**, *5* (1), 3–8. https://doi.org/10.1017/S0954102093000021.

(26) Blum, J. D.; Johnson, M. W.; Gleason, J. D.; Demers, J. D.; Landis, M. S.; Krupa, S. Chapter 16 - Mercury Concentration and Isotopic Composition of Epiphytic Tree Lichens in the Athabasca Oil Sands Region. In *Alberta Oil Sands*; Percy, K. E., Ed.; Developments in Environmental Science; Elsevier, 2012; Vol. 11, pp 373–390. https://doi.org/10.1016/B978-0-08-097760-7.00016-0.

(27) Carignan, J.; Estrade, N.; Sonke, J. E.; Donard, O. F. X. Odd Isotope Deficits in Atmospheric Mercury Measured in Lichens. *Environmental Science & Technology* **2009**, *43*, 5560–5564.

(28) Estrade, N.; Carignan, J.; Donard, O. F. X. Isotope Tracing of Atmospheric Mercury Sources in an Urban Area of Northeastern France. *Environmental Science and Technology* **2010**, *44*, 6062–6067.

(29) Enrico, M.; Le Roux, G.; Marusczak, N.; Heimbürger, L.-E.; Claustres, A.; Fu, X.; Sun, R.; Sonke, J. E. Atmospheric Mercury Transfer to Peat Bogs Dominated by Gaseous Elemental Mercury Dry Deposition. *Environmental Science & Technology* **2016**. https://doi.org/10.1021/acs.est.5b06058.

(30) Enrico, M.; Le Roux, G.; Heimburger, L.-E.; Van Beek, P.; Souhaut, M.; Chmeleff, J.; Sonke, J. E. Holocene Atmospheric Mercury Levels Reconstructed from Peat Bog Mercury Stable Isotopes. *Environmental Science & Technology* **2017**, *51* (11), 5899–5906. https://doi.org/10.1021/acs.est6b05804.

(31) New, M.; Lister, D.; Hulme, M.; Makin, I. A High-Resolution Data Set of Surface Climate over Global Land Areas. *Climate Research* **2002**, *21*, 1–25.

(32) NASA. Goddard Institute for Space Studies - Climate Model Simulations: Past Climate Change and Future Climate Predictions http://aom.giss.nasa.gov/.

(33) Blum, J. D.; Bergquist, B. A. Reporting of Variations in the Natural Isotopic Composition of Mercury. *Analytical and Bioanalytical Chemistry* **2007**, *388*, 353–359.

(34) Estrade, N.; Carignan, J.; Sonke, J. E.; Donard, O. F. X. Measuring Hg Isotopes in Bio-Geo-Environmental Reference Materials. *Geostandard and Geoanalysis Research* **2010**, *34* (1), 79–93.

(35) AMAP. *AMAP Assessment 2011: Mercury in the Arctic.*; Arctic Monitoring and Assessment Programme (AMAP): Oslo, Norway, 2011.

(36) Schroeder, W. H.; Anlauf, K. G.; Barrie, L. A.; Lu, J. Y.; Steffen, A.; Schneeberger, D. R.; Berg, T. Arctic Springtime Depletion of Mercury. *Nature* **1998**, *394*, 331–332.

(37) Steffen, A.; Douglas, T.; Amyot, M.; Ariya, P.; Aspmo, K.; Berg, T.; Bottenheim, J.; Brooks, S.; Cobbett, F.; Dastoor, A.; Dommergue, A.; Ebinghaus, R.; Ferrari, C.; Gardfeldt, K.; Goodsite, M. E.; Lean, D.; Poulain, A. J.; Scherz, C.; Skov, H.; Sommar, J.; Temme, C. A Synthesis of Atmospheric Mercury Depletion Event Chemistry in the Atmosphere and Snow. *Atmospheric Chemistry and Physics* **2008**, *8*, 1445–1482.

(38) Lindberg, S. E.; Brooks, S.; Lin, C.-J.; Scott, K. J.; Landis, M. S.; Stevens, R. K.; Goodsite, M.; Richter, A. Dynamic Oxidation of Gaseous Mercury in the Arctic Troposphere at Polar Sunrise. *Environ. Sci. Technol.* **2002**, *36* (6), 1245–1256. https://doi.org/10.1021/es0111941.

(39) Carignan, J.; Sonke, J. E. The Effect of Atmospheric Mercury Depletion Events on the Net Deposition Flux Around Hudson Bay, Canada. *Atmospheric Environment* **2010**, *44*, 4372–4379.

(40) St Pierre, K. A.; St Louis, V. L.; Kirk, J. L.; Lehnherr, I.; Wang, S.; La Farge, C. Importance of Open Marine Waters to the Enrichment of Total Mercury and Monomethylmercury in Lichens in the Canadian High Arctic. *Environmental Science & Technology* **2015**, *49* (10), 5930–5938. https://doi.org/10.1021/acs.est.5b00347.

(41) Ares, A.; Aboal, J.; Carballeira, A.; Fernández, J. A. Do Moss Bags Containing Devitalized Sphagnum Denticulatum Reflect Heavy Metal Concentrations in Bulk Deposition? *Ecological Indicators* **2015**, *50*, 90–98. https://doi.org/10.1016/j.ecolind.2014.10.030.

(42) Bergquist, B. A.; Blum, J. D. The Odds and Evens of Mercury Isotopes: Applications of Mass-Dependent and Mass-Independent Isotope Fractionation. *Elements* **2009**, *5*, 353–357.

(43) Kwon, S. Y.; Blum, J. D.; Yin, R.; Tsui, M. T.-K.; Yang, Y. H.; Choi, J. W. Mercury Stable Isotopes for Monitoring the Effectiveness of the Minamata Convention on Mercury. *Earth-Science Reviews* **2020**, *203*, 103111. https://doi.org/10.1016/j.earscirev.2020.103111.

(44) Shah, V.; Jaegle, L.; Gratz, L. E.; Ambrose, J. L.; Jaffe, D. A.; Selin, N. E.; Song, S.; Campos, T. L.; Flocke, F. M.; Reeves, M.; Stechman, D.; Stell, M.; Festa, J.; Stutz, J.; Weinheimer, A. J.; Knapp, D. J.; Montzka, D. D.; Tyndall, G. S.; Apel, E. C.; Hornbrook, R. S.; Hills, A. J.; Riemer, D. D.; Blake, N. J.; Cantrell, C. A.; Mauldin, R. L. Origin of Oxidized Mercury in the Summertime Free Troposphere over the Southeastern US. *Atmospheric Chemistry and Physics* **2016**, *16* (3), 1511–1530. https://doi.org/10.5194/acp-16-1511-2016.

(45) Fu, X. Mass-Independent Fractionation of Even and Odd Mercury Isotopes during Atmospheric Mercury Redox Reactions. *Environ. Sci. Technol* **2021**. https://doi.org/10.1021/acs.est.1c02568.

(46) Kritee, K.; Motta, L. C.; Blum, J. D.; Tsui, M. T.-K.; Reinfelder, J. R. Photomicrobial Visible Light-Induced Magnetic Mass Independent Fractionation of Mercury in a Marine Microalga. *ACS Earth Space Chem.* **2018**, *2* (5), 432–440. https://doi.org/10.1021/acsearthspacechem.7b00056.

(47) Sherman, L. S.; Blum, J. D.; Johnson, K. P.; Keeler, G. J.; Barres, J. A.; Douglas, T. A. Mass-Independent Fractionation of Mercury Isotopes in Arctic Snow Driven by Sunlight. *Nature Geoscience* **2010**, *3*, 173–177.

(48) Yang, X.; Jiskra, M.; Sonke, J. E. Experimental Rainwater Divalent Mercury Speciation and Photoreduction Rates in the Presence of Halides and Organic Carbon. *Science of The Total Environment* **2019**, *697*, 133821. https://doi.org/10.1016/j.scitotenv.2019.133821.

(49) Demers, J. D.; Blum, J. D.; Zak, D. R. Mercury Isotopes in a Forested Ecosystem: Implications for Air-Surface Exchange Dynamics and the Global Mercury Cycle. *Global Biogeochemical Cycles* **2013**, *27* (1), 222–238. https://doi.org/10.1002/gbc.20021.

(50) Barre, J. P. G.; Deletraz, G.; Sola-Larrañaga, C.; Santamaria, J. M.; Bérail, S.; Donard, O. F. X.; Amouroux, D. Multi-Element Isotopic Signature (C, N, Pb, Hg) in Epiphytic Lichens to Discriminate Atmospheric Contamination as a Function of Land-Use Characteristics (Pyrénées-Atlantiques, SW France). *Environmental Pollution* **2018**, *243*, 961–971. https://doi.org/10.1016/j.envpol.2018.09.003.

(51) Ferreira Araujo, B.; et al.; Sonke, J. E. Mercury Isotope Evidence for Arctic Summertime Re-Emission of Mercury from the Cryosphere. *EarthArXiv*. 2022.

(52) Barre, J. P. G.; Queipo-Abad, S.; Sola-Larrañaga, C.; Deletraz, G.; Bérail, S.; Tessier, E.; Elustondo Valencia, D.; Santamaría, J. M.; de Diego, A.; Amouroux, D. Comparison of the Isotopic Composition of Hg and Pb in Two Atmospheric Bioaccumulators in a Pyrenean Beech Forest (Iraty Forest, Western Pyrenees, France/Spain). *Frontiers in Environmental Chemistry* **2020**, *1*, 14. https://doi.org/10.3389/fenvc.2020.582001.

(53) Olson, C. L.; Jiskra, M.; Sonke, J. E.; Obrist, D. Mercury in Tundra Vegetation of Alaska: Spatial and Temporal Dynamics and Stable Isotope Patterns. *Sci. Total Environ* **2019**, *660*, 1502–1512.

Figures and Tables

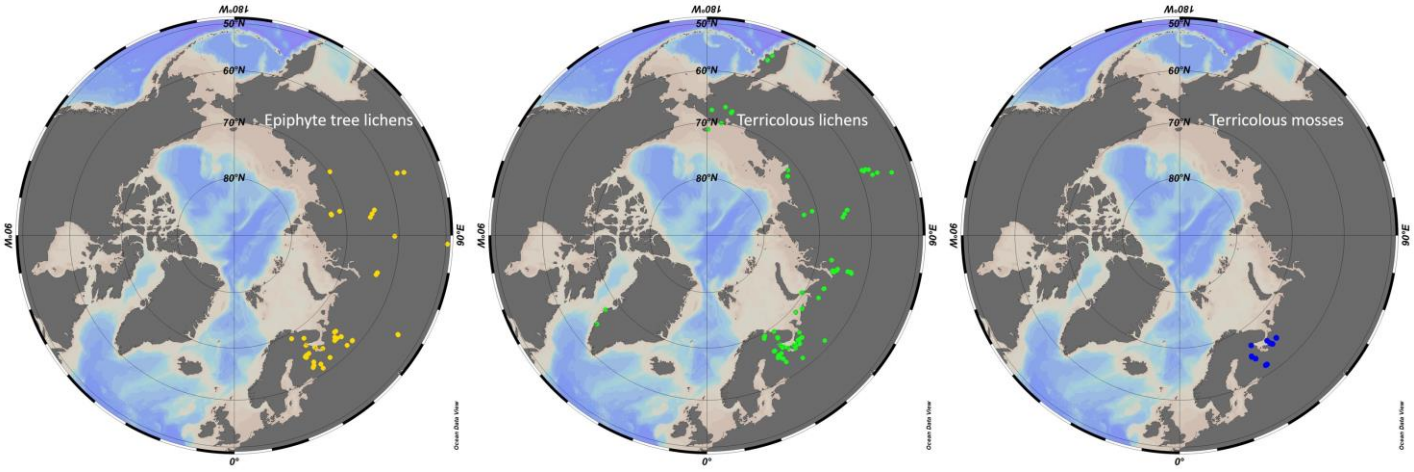

Figure 1. Overview of geographical sample origin for epiphyte tree lichens (left, yellow circles), terricolous lichens (middle, green circles), and terricolous mosses (right, blue circles).

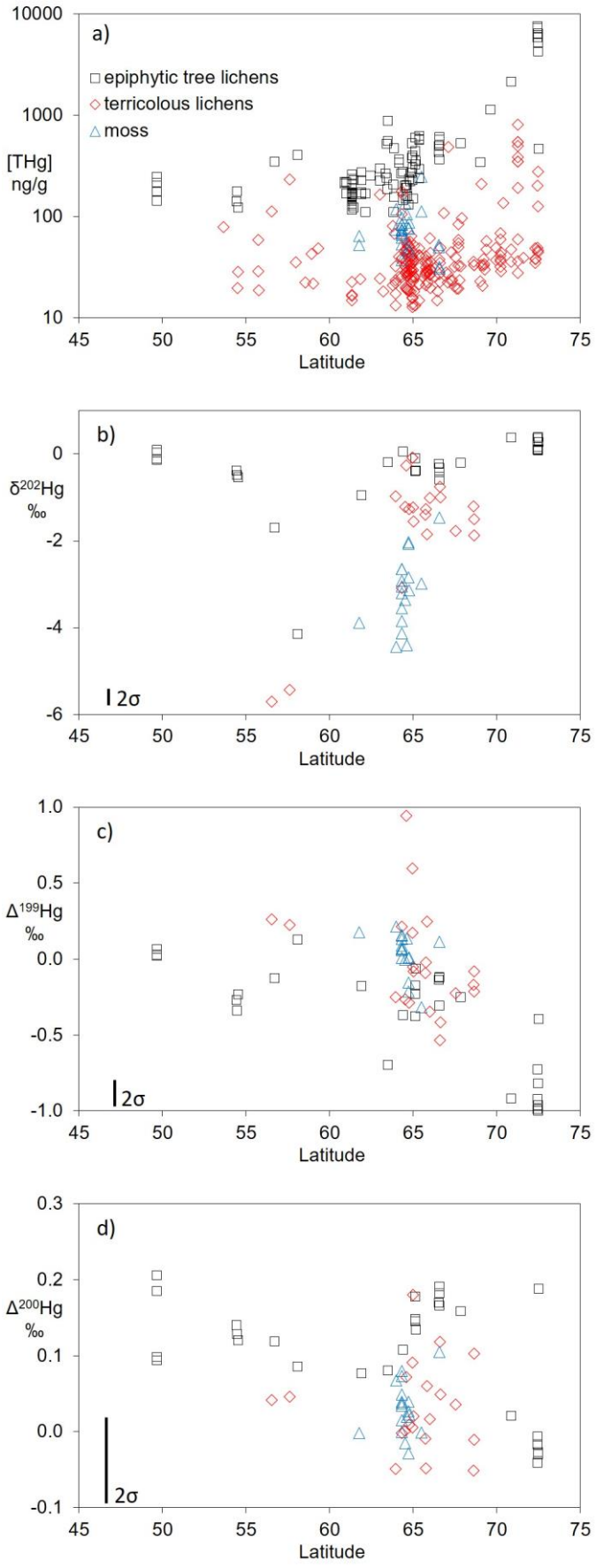

421

422 Figure 2. Latitudinal variation of total Hg (THg, a), and Hg isotopic composition (b, c, d) for epiphyte tree
423 lichens (black squares), terricolous lichens (red diamonds), and terricolous mosses (blue triangles).

424

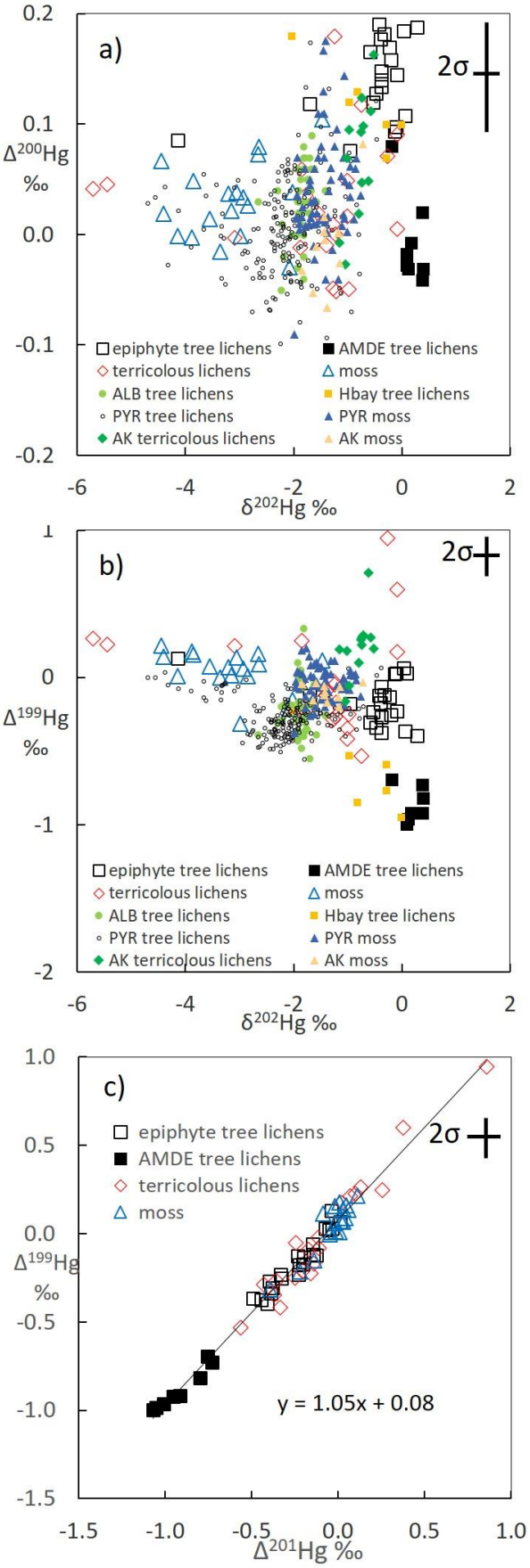

Figure 3. Comparison of Eurasian lichen and moss δ^{202}Hg, Δ^{199}Hg, and Δ^{200}Hg with northern hemisphere lichen and moss data [26,27,29,50,52,53]. Double-sided 2σ uncertainties are indicated in the panels. ALB, Alberta, PYR, Pyrenees, AK, Alaska, HBay, Hudson Bay.

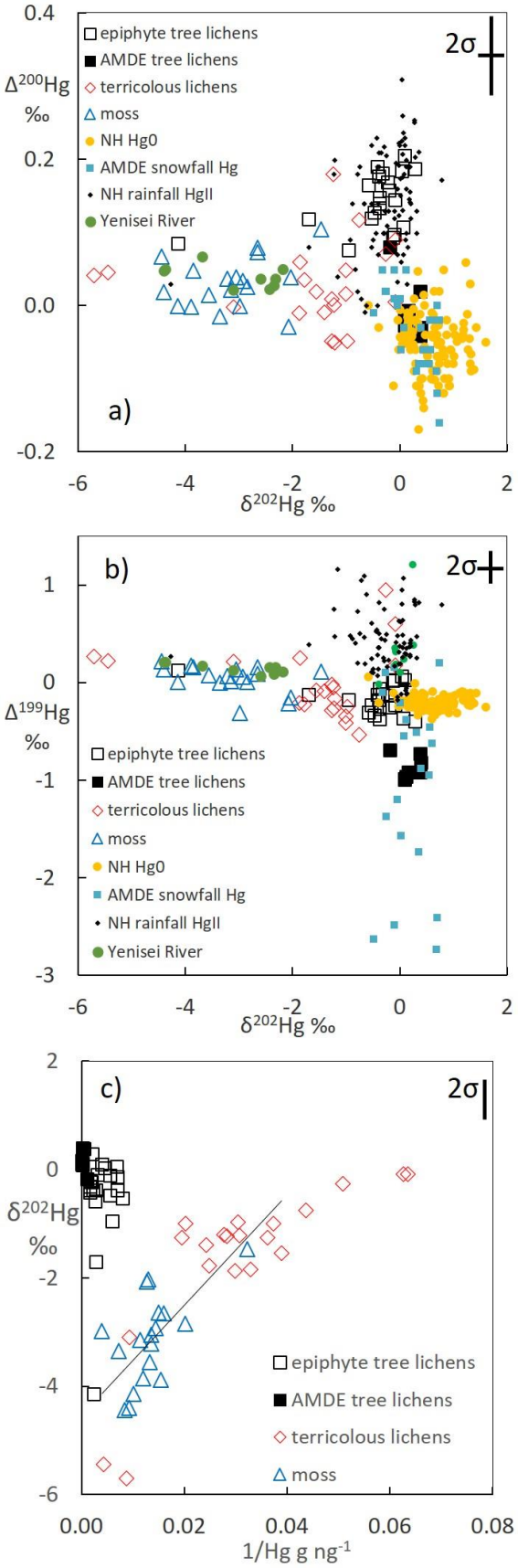

Figure 4. a,b) Comparison of Eurasian lichen and moss $\delta^{202}Hg$, $\Delta^{199}Hg$, and $\Delta^{200}Hg$ with northern hemisphere atmospheric Hg^0 and Hg^{II} data (see compilation by [9], and with AMDE associated snowfall observations [19,47]. c) Source mixing diagram based on THg concentrations and $\delta^{202}Hg$. Double-sided 2σ uncertainties are indicated in the panels.

Table 1. THg concentration and Hg isotope composition of epiphyte lichens, terricolous lichens and moss. Epiphyte lichens are separated into two groups, one affected by atmospheric Hg depletion events (AMDEs) in coastal regions, and the other not (in-land sites >300km from the Arctic Ocean coast). Q25 and Q75 refer to the 25th and 75th percentiles of data variability respectively; n, number of observations; min, minimum value; max, maximum value.

	lichen	**AMDE lichen**	**lichen**	**moss**
THg (ng g^{-1})	**epiphyte**	**epiphyte**	**terricolous**	**terricolous**
n	105	7	191	28
min	112	2185	13	31
max	1159	7667	821	250
median	243	5987	35	74
Q25	172	4320	26	53
Q75	411	7424	49	87
δ^{202}Hg (‰)				
n	22	7	20	18
median	-0.35	0.16	-1.25	-3.10
Q25	-0.49	0.09	-1.83	-3.86
Q75	-0.11	0.37	-0.99	-2.65
Δ^{199}Hg (‰)				
median	-0.18	-0.92	-0.09	0.07
Q25	-0.31	-0.99	-0.26	0.00
Q75	-0.04	-0.82	0.22	0.14
Δ^{200}Hg (‰)				
median	0.14	-0.03	0.02	0.03
Q25	0.11	-0.03	-0.01	0.00
Q75	0.18	-0.01	0.06	0.05
Δ^{201}Hg (‰)				
median	-0.23	-0.95	-0.15	0.00
Q25	-0.39	-1.05	-0.31	-0.06
Q75	-0.11	-0.80	0.09	0.03